Computational Materials Science 172 (2020) 109345

Contents lists available at ScienceDirect

Computational Materials Science

journal homepage: www.elsevier.com/locate/commatsci

The formations of C_2 species and CH_4 over the Co_2C catalyst in Fischer-Tropsch synthesis: The effect of surface termination on product selectivity

Ping Liu[a], Danli Liang[b], Riguang Zhang[b], Baojun Wang[b,*]

[a] State Key Laboratory of Coal Conversion, Institute of Coal Chemistry, Chinese Academy of Science, Taiyuan 030001, Shanxi, PR China
[b] Key Laboratory of Coal Science and Technology of Ministry of Education and Shanxi Province, Taiyuan University of Technology, Taiyuan 030024, Shanxi, PR China

ARTICLE INFO

Keywords:
Co_2C catalyst
Fischer-Tropsch synthesis
Surface termination
Product selectivity
Density functional theory

ABSTRACT

Co_2C is considered to be the active phase for the formations of C_{2+} species (C_{2+} oxygenates and hydrocarbons) and CH_4 in Fischer-Tropsch synthesis (FTS), in this study, the mainly exposed (1 0 1) surface is employed to investigate the effects of C- and Co-termination Co_2C surfaces on FTS selectivity (C_2 species and CH_4); here, the density functional theory calculations are carried out. The results show that on the C-Co_2C(1 0 1) surface, CH_3 is the main form of CH_x species, CH_4 formed by CH_3 hydrogenation is the main C_1 species; then, CH_3CH_2 formed by CH_2 coupling with CH_3 is the main C_2 species; however, the formation of C_1 species CH_4 is more favorable in kinetics than that of C_2 species CH_3CH_2. Whereas on the Co-Co_2C(1 0 1) surface, CH is the main form of CH_x species, C_2H_2 formed by CH self-coupling is the main C_2 species, CH_4 formation is very difficult. For the C_2 species formation, both C- and Co-Co_2C(1 0 1) surfaces prefer to form the hydrocarbons rather than the oxygenates. Thus, either the C- or Co-termination Co_2C(1 0 1) surface is in favor of hydrocarbons formation (CH_4 and C_{2+} hydrocarbons), the surface termination of Co_2C(1 0 1) surface affects the product selectivity of FTS reactions, and the exposed Co-terminated surface prefers to form C_{2+} hydrocarbons. As a result, adjusting the surface termination of Co_2C catalysts can tune the selectivity of FTS reactions.

1. Introduction

Recently, Zhong et al. [1,2] showed that the formation of Co_2C nanoprisms in a parallelepiped morphology with a pair of rhomboid faces can contribute to the synthesis of C_2–C_4 olefins in Fischer-Tropsch synthesis (FTS) reaction, in which the mainly exposed Co_2C(1 0 1) and (0 2 0) crystal facets presents high selectivity of lower olefins and the low selectivity of CH_4. Meanwhile, previous experimental and theoretical studies [2–6] also found that the (1 0 1) surface is the most stable and the mainly exposed surface among all Co_2C low index surfaces.

For Co_2C(1 0 1) surface, two types of surface terminations exist, the C-terminated and Co-terminated surfaces. The difference of surface termination may lead to different catalytic performances and product distribution toward the target reaction. For example, for the MoS_2(1 0 0) surface [7,8], CO activation and hydrogenation on the Mo-termination surface is more favorable than that on the S-termination surface. For CO adsorption and activation over the Mo_2C(1 0 0) [9] and Mo_2C(0 0 1) [10–13] surfaces, the Mo-termination surface prefers to be dissociative adsorption instead of its molecular adsorption over the C-termination surface. Kim et al. [14] studied the effect of Mo_2C(1 0 0) surface termination on propanoic acid deoxygenation, suggesting that the Mo-termination surface favors hydrodeoxygenation pathway, whereas the C-termination surface prefers to be the decarboxylation pathway, namely, Mo_2C(1 0 0) surface termination can alter the reaction pathways. Carlos et al. [15] studied the adsorption of acetylene and ethylene on the C- and Mo-terminations of β-Mo_2C(1 0 0), indicating that the Mo-termination surface is not suitable for hydrogenation of acetylene and ethylene due to the strong adsorption energies, however, the C-termination of β-Mo_2C(1 0 0) surface is favorable for the hydrogenation.

Above results show that the surface termination of metal carbide and metal sulfide can alter the reaction pathway, and therefore change catalytic activity and selectivity toward the specific reaction, namely, the catalytic performance of metal carbide and metal sulfide is sensitive to its corresponding surface termination. Previous experimental and theoretical studies [3,16] have investigated the effect of Co_2C crystal facets on FTS selectivity over the Co-terminated (1 0 1), (1 1 0), (1 1 1), and (0 2 0), however, the selectivity over the exposed C-terminated surfaces are still unclear. Especially, for the mainly exposed (1 0 1) surface, the effect of Co- and C-termination on the reaction pathway and FTS selectivity is still unknown, it is necessary to understand the role of Co_2C(1 0 1) surface termination at a molecular level. On the

* Corresponding author.
E-mail addresses: wangbaojun@tyut.edu.cn, wbj@tyut.edu.cn (B. Wang).

https://doi.org/10.1016/j.commatsci.2019.109345
Received 25 October 2018; Received in revised form 9 October 2019; Accepted 10 October 2019

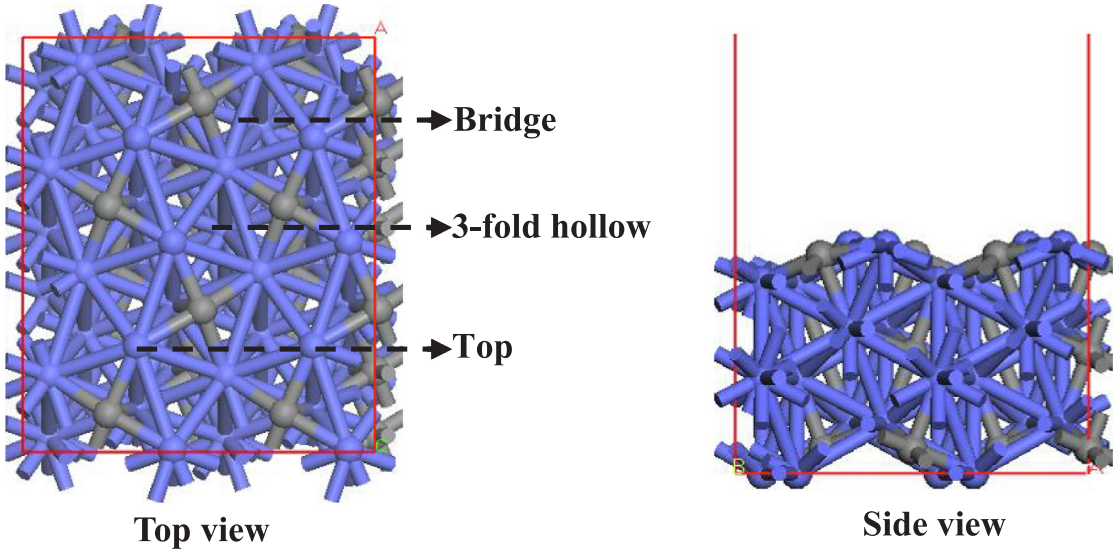

(a) C-Co_2C(101) surface

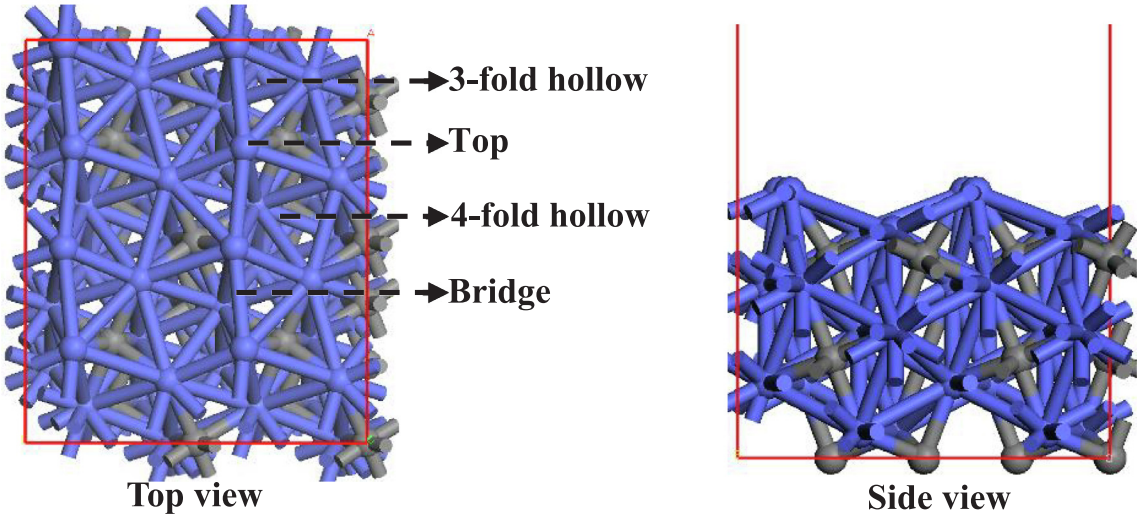

(b) Co-Co_2C(101) surface

Fig. 1. The surface morphology and its adsorption sites of C-Co_2C(1 0 1) and Co-Co_2C(1 0 1).

other hand, Li et al. [3,4] found that different Co_2C surface termination can provide CO non-dissociative adsorption and CO hydrogen-assisted dissociation to CH, followed by its hydrogenation to CH_x(x = 2,3) species, indicating that CH_x(x = 1–3), CO, and H are the abundant species to identify FTS selectivity.

In this study, aiming at shedding light on the surface termination effects of mainly exposed Co_2C(1 0 1) on FTS selectivity, as well as the origin of the promising catalytic performance of Co_2C(1 0 1) surface for promoting lower olefins formation and inhibiting CH_4 mentioned in the previous studies [2,3], the density functional theory (DFT) calculations are resorted to investigate the formation mechanism of lower olefins (C_2H_x as an example) and of methane over the C- and Co-terminated Co_2C(1 0 1) surfaces. Since CO is the abundant reactant in FTS reaction, CO insertion into CH_x to C_2 oxygenates (C_2H_xO as an example) is also examined. The achieved insights are expected to provide a clue for designing Co_2C catalyst with high selectivity in FTS reactions.

2. Computational models and methods

2.1. Surface models

Co_2C(1 0 1) has the lowest surface energy among low index surfaces and is the mainly exposed surface [4–6]. Meanwhile, different CO/H_2 ratios affect the exposed termination of Co_2C catalyst in FTS reactions, in CO-rich atmosphere, Co_2C catalyst exposed the C-terminated surface [4,5], whereas the in hydrogen-rich atmosphere, the Co-terminated surfaces are exposed [3,5]. Thus, this work examined two types of Co_2C(1 0 1) surface terminations: the C-rich and Co-rich surfaces, which are named as C-Co_2C(1 0 1) and Co-Co_2C(1 0 1), respectively (see Fig. 1).

On the C-Co_2C(1 0 1) surface (see Fig. 1(a)), C atoms occupy the 4-fold hollow Co site; three adsorption sites exist: Top, Bridge, and 3-fold hollow sites. On the Co-Co_2C(1 0 1) surface (Fig. 1(b)), C atoms only appear at the third layer; four adsorption sites exist: Top, Bridge, 3-fold

Table 1
Adsorption free energies (G_{ads}) at 493 K and the key structural parameters of the most stable configurations for all adsorbed species involved in the reactions related to CH_x(x = 1–3) species on the C-Co_2C(1 0 1) surface.

Species	Adsorption site	$d_{Co\text{-}C}$/Å	G_{ads}/eV
H	3-fold	Co-H: 1.678, 1.706, 1.851	−2.57(−2.57)*
C	3-fold	1.745, 1.779, 1.840	−6.31(−6.31)
CO	top	1.741	−0.92(−1.70)
CH	3-fold	1.857, 1.818, 1.927	−6.09(−6.28)
CH_2	3-fold	1.894, 1.936, 2.099; Co-H: 1.717	−3.20(−3.39)
CH_3	bridge	2.000, 2.202; Co-H: 1.844	−1.76(−1.95)
CH_4	top	2.653; Co-H: 2.132	−0.06(−0.06)
C_2H_2	(β-C)top-(α-C)bridge	α:1.889, 2.345; β:1.850	−1.22(−1.41)
CH_2CH	(β-C)top-(α-C)bridge	α: 1.902, 2.029; β: 2.082	−2.73(−2.92)
CH_3CH	(α-C)bridge	α: 1.939, 1.924	−3.62(−3.81)
C_2H_4	(β-C)top-(α-C)bridge	α: 2.125, 2.224; β: 1.999; Co-(α)H: 1.964	−0.87(−1.06)
CH_3CH_2	(α-C)bridge	α: 2.219, 2.033; Co-(α)H: 1.856	−1.45(−1.63)
C_2H_6	away from the surface		−0.01(−0.05)
CHCO	(β-C) bridge-(α-C)top	α:1.969; β:1.910, 2.012	−2.88(−3.07)
CH_2CO	(β-C) bridge-(α-C)top	α:1.819; β:2.198, 2.034	−1.04(−1.23)
CH_3CO	(α-C)top	α:1.831; Co-O: 2.001	−2.37(−2.56)

* The values in the parentheses are the adsorption energy at 0 K.

Table 2
Adsorption free energies (G_{ads}) at 493 K and the key structural parameters of the most stable configurations for all adsorbed species involved in the reactions related to CH_x(x = 1–3) species on the Co-Co_2C(1 0 1) surface.

Species	Adsorption site	$d_{Co\text{-}C}$/Å	G_{ads}/eV
H	3-fold	Co-H: 1.749, 1.720, 1.803	−3.03(−2.94)
C	4-fold	1.870, 1.871, 1.910, 1.808	−8.02(−8.08)
CO	3-fold	1.938, 2.0361, 1.936	−1.28(−2.08)
CH	4-fold	1.906, 1.953, 1.954, 2.076	−6.82(−7.11)
CH_2	3-fold	1.930, 1.974, 1.938; Co-H: 1.694	−4.45(−4.64)
CH_3	bridge	2.032, 2.091; Co-H: 1.866	−2.18(−2.36)
CH_4	top	2.392; Co-H: 2.004, 2.055	−0.22(−0.22)
C_2H_2	(β-C)bridge-(α-C)3-fold	α: 2.061, 2.008, 1.933; β: 2.036, 1.929	−2.21(−2.39)
CH_2CH	(β-C)top-(α-C)3-fold	α: 1.962, 2.036, 1.962;β: 2.068; Co-H: 1.760	−3.21(−3.40)
CH_3CH	(β-C)top-(α-C)3-fold	α: 1.914, 1.977, 1.939;β: 2.209; Co-(α)H: 1.745; Co-(β)H: 1.761	−3.86(−4.04)
C_2H_4	(β-C)3-fold-(α-C)top	α: 1.987; β: 2.119, 2.294, 2.075; Co-(β)H: 1.872	−1.12(−1.31)
CH_3CH_2	(β-C)top-(α-C)3-fold	α: 2.087, 2.254, 2.113;β: 2.119; Co-(α)H: 2.098, 1.815; Co-(β)H: 1.745	−2.00(−2.19)
C_2H_6	top	Co-H: 1.942	−0.14(−0.18)
CHCO	4-fold	α:2.026, 1.959; β:2.117, 1.968, 2.030	−3.41(−3.60)
CH_2CO	(β-C)(α-C)bridge	α:2.563, 1.775; β:2.044, 2.506; Co-O: 2.051	−1.72(−1.91)
CH_3CO	(β-C)top-(α-C)3-fold	α: 1.969, 1.980, 2.448;β: 2.285; Co-O: 1.900; Co-(β)H: 1.828	−2.53(−2.72)

*The values in the parentheses are the adsorption energy at 0 K.

hollow and 4-fold hollow sites. Since C atoms occupies the 4-fold hollow site of C-Co_2C(1 0 1), this surface has fewer active sites compared to Co-Co_2C(1 0 1) surface, which will affects the activity and selectivity of FTS reaction [17,18].

A $p(2 \times 2)$ supercell is used for both C-Co_2C(1 0 1) and Co-Co_2C(1 0 1) surfaces, which include 48 Co and 24 C atoms, six Co layer slabs and three C layer slabs, the topmost four Co layers including C atoms and the adsorbates are fully relaxed in all calculations, and the bottom two Co layers including C atoms are fixed. A 15 Å vacuum layer is inserted to avoid the interactions of periodic images between the periodically repeated slabs.

2.2. Computational methods

The periodic density functional theory (DFT) calculations are performed using the Vienna Ab Initio Simulation Package (VASP) [19–21]. The plane-wave basis sets expanded valence states of one-electron is the projector-augmented wave (PAW) [22–24] method with a cutoff energy of 400 eV. The exchange correlation energy of the electrons is treated with the generalized gradient approximation (GGA) in the Perdew-Wang 91 (PW91) formalism [25,26]. Electronic convergence is set to 10^{-4} eV, and the forces converged to 0.04 eV $Å^{-1}$. A 3 × 3 × 1 k-point is performed for sampling the Brillouin-zone integration to calculate surface slab.

The transition states is calculated by the Climbing-Image Nudged Elastic Band method (CI-NEB) [27,28] and Dimer method [29,30], and the transition state structures would be converged with the forces for all atoms are less than 0.04 eV/Å. The transition states have the only one imaginary frequency, as listed in Table S1. The adsorption, activation and reaction free energies are calculated at 493 K (see details in the Part 2 of Supplementary Material).

3. Results and discussion

Firstly, the surface energy of the C- and Co-termination Co_2C(1 0 1) surfaces are calculated. The results showed that the surface energies of C- and Co-termination Co_2C(1 0 1) surfaces are 33.2 and 32.2 J/m^2, respectively, suggesting that the Co-termination surface is relatively stable compared to C-termination surface, while the difference of the surface energy between Co- and C termination surfaces is only 1.0 J/m^2; thus, the Co- and C- termination Co_2C(1 0 1) surfaces are considered in this study.

Then, it is widely accepted that for syngas conversion to C_2 species, two key steps exist, one is the formation of key CH_x intermediates by CO activation; the other is the formation of C_2 species via the CO/CHO insertion into CH_x(x = 1–3), the coupling of CH_x species, as well as methane formation via CH_x hydrogenation. Since this study focuses on the investigation about the effect of Co_2C catalyst surface termination

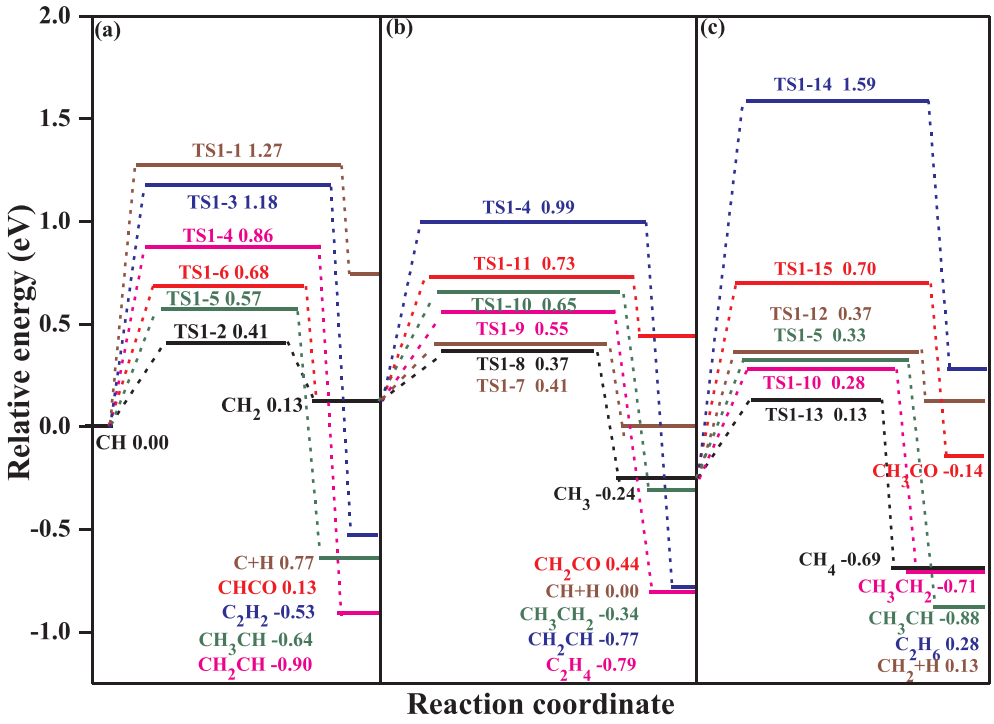

Fig. 2. The potential energy profile of Gibbs free energy (493 K) for the all reactions related to CH_x(x = 1–3) species on the C-Co_2C(1 0 1) surface, the corresponding structures of initial states (ISs), transition states (TSs) and final states (FSs) are shown in Fig. 3.

on the selectivity of the products between C_2 species and CH_4 in FTS reactions, the formation of key CH_x intermediates by CO activation is not considered in this study. Thus, starting from all possible CH_x(x = 1–3) monomer, C_1 species (CH_4 and C) formed by CH_x(x = 1–3) hydrogenation and dissociation, C_2 species (C_2H_x and C_2H_xO) formed by CO insertion into CH_x(x = 1–3) and CH_x coupling with CH_y(x, y = 1–3) are considered on the C- and Co-Co_2C(1 0 1) surfaces.

The adsorption free energies (G_{ads}) at 493 K and the key structural parameters of the most stable configurations for the species involved in the reactions related to CH_x(x = 1–3) species on the C- and Co-Co_2C(1 0 1) surfaces are presented in Tables 1 and 2, respectively. The results show that the adsorption free energies for the species over Co-Co_2C(1 0 1) are higher than those over C-Co_2C(1 0 1).

3.1. The reactions related to CH_x(x = 1–3) species on the C-Co_2C(1 0 1)

3.1.1. The related reactions of CH species

As presented in Fig. 2(a), CH hydrogenation to CH_2 is the most favored with the smallest activation free energy of 0.41 eV, it is endothermic by 0.13 eV. The second favored reaction is CH + CH_3 coupling to CH_3CH with the activation and reaction free energies of 0.57 and −0.64 eV. The third and fourth reactions correspond to CO insertion into CH to CHCO and CH + CH_2 coupling to CH_2CH with the activation free energies of 0.68 and 0.86 eV, respectively; the corresponding reaction free energies are 0.13 and −0.90 eV, respectively. The last two reactions are CH self-coupling to C_2H_2 and CH dissociation into C, which have the higher activation free energies of 1.18 and 1.27 eV with the reaction free energies of −0.53 and 0.77 eV, respectively.

On the other hand, the effective barrier (E_{eff}) [31–34] (see Table 3 and the detailed descriptions in the Part 3 of Supplementary Material) is used to quantitatively evaluate FTS activity, which contains the coverage of C_1 species (CH_x, CO and H) and the available sites (θ_{CHx}, θ_{CO}, θ_H and θ_*). The smaller the value of E_{eff} is, the higher the activity of the reaction is. For the related reactions of CH species (Table 3), the effective barrier of CH hydrogenation to CH_2 (0.45 eV) is the smallest, and the second is still CH coupling with CH_3 to CH_3CH (0.99 eV).

Above results show that CH species is in favor of its hydrogenation to CH_2 in kinetics over the C-Co_2C(1 0 1) surface.

3.1.2. The related reactions of CH_2 species

As shown in Fig. 2(b), both CH_2 hydrogenation to CH_3 and its dissociation to CH are two parallel and most favorable reactions (0.24 and 0.28 eV) due to the small difference of activation free energy. Moreover, these two reactions also have the lower effective barrier of 0.42 and 0.44 eV (see Table 3), respectively. Further, CH_3 is thermodynamically stable than CH and CH_2, as a result, CH_2 is dominantly hydrogenated to CH_3 over the C-Co_2C(1 0 1) surface.

3.1.3. The related reactions of CH_3 species

As illustrated in Fig. 2(c), CH_3 hydrogenation to CH_4 has the lowest activation free energy of 0.37 eV, and it is exothermic by 0.45 eV. The second is CH_3 coupling with CH_2 to CH_3CH_2 with the activation and reaction free energies of 0.52 and −0.47 eV, respectively. The third is CH_3 coupling with CH to CH_3CH with the activation and reaction free energies of 0.57 and −0.64 eV, respectively. The fourth is CH_3 dissociation into CH_2 with the activation and reaction free energies of 0.61 and 0.37 eV, respectively. Similarly, the E_{eff} value of 0.67 eV for CH_3 hydrogenation to CH_4 (see Table 3) is the smallest. Therefore, CH_3 hydrogenation to CH_4 is favored in kinetics over the C-Co_2C(1 0 1) surface.

3.2. The reactions related to CH_x(x = 1–3) species on the Co-Co_2C(1 0 1) surface

Our previous studies [16] have probed into the related reactions of CH_x(x = 1–3) species on the Co-Co_2C(1 0 1) surface. As shown in Fig. 4(a), CH self-coupling to C_2H_2 with the lowest activation free energy of 0.37 eV is more favorable in kinetics than other related reactions of CH species; meanwhile, CH self-coupling to C_2H_2 has the smallest effective barrier of 0.93 eV. As shown in Fig. 4(b), CH_2

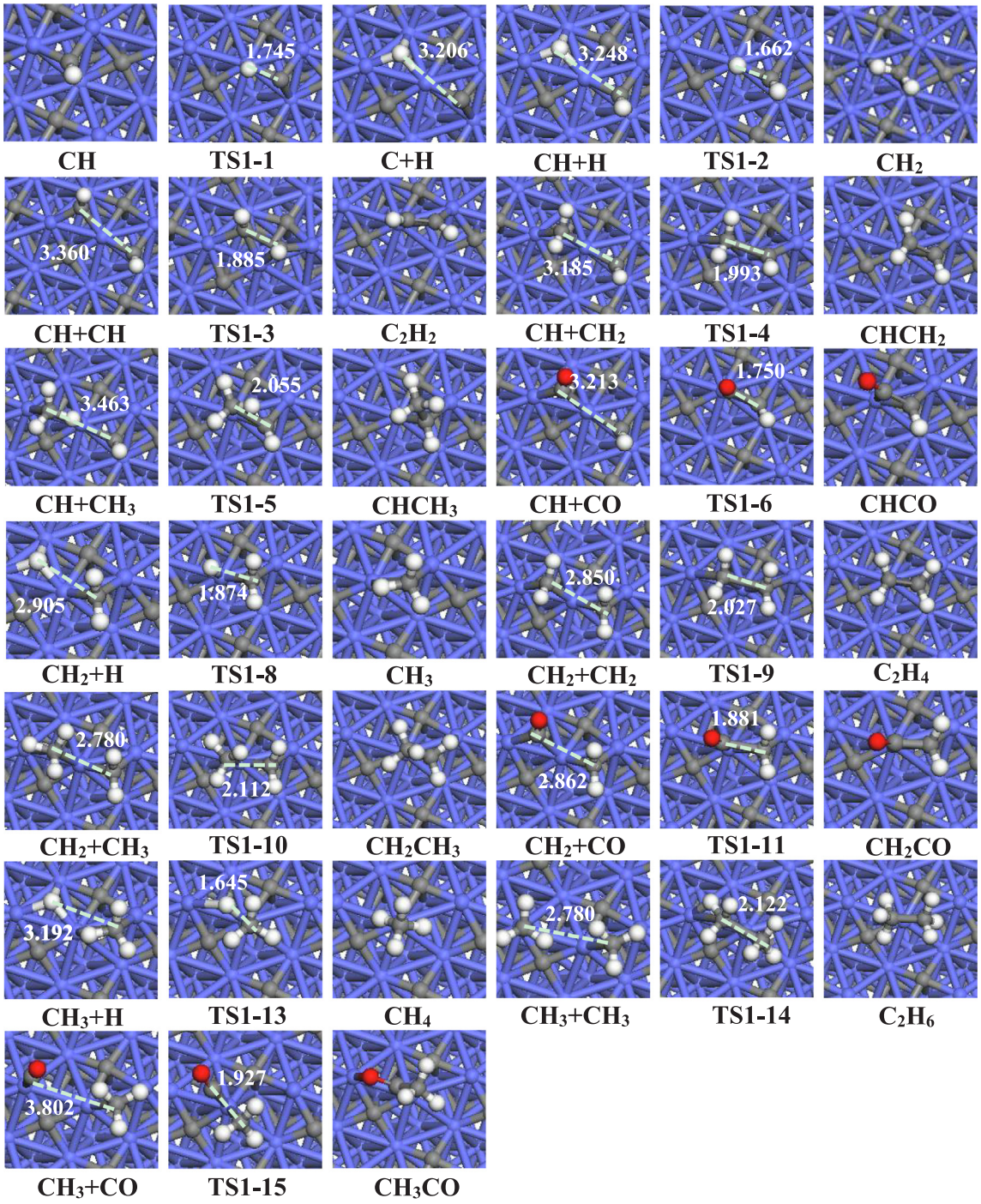

Fig. 3. The structures of initial states (ISs), transition states (TSs) and final states (FSs) for the all reactions related to CH_x(x = 1–3) species on the C-Co_2C(1 0 1) surface. Co, C, H and O atoms are shown in the blue, grey, white and red balls, respectively. Bond length is in Å. (For interpretation of the references to colour in this figure legend, the reader is referred to the web version of this article.)

dissociation into CH has the lowest activation free energy of 0.10 eV with the effective barrier of 0.73 eV. As shown in Fig. 4(c), CH_3 dissociation into CH_2 has the lowest activation free energy of 0.37 eV with the effective barrier of 1.08 eV.

3.3. General discussions

3.3.1. The effects of Co_2C(1 0 1) surface termination on FTS selectivity

As mentioned above, for the C-Co_2C(1 0 1), once CH and CH_2 species are formed, both species is more easier to be hydrogenated to the favored monomer CH_3. Then, CH_3 hydrogenation to CH_4 is more favorable than CO insertion into CH_3 or its self-coupling to C_2 oxygenates and hydrocarbons, respectively. Hence, the C-Co_2C(1 0 1) surface can promote CH_x hydrogenation to CH_4, which exhibits high selectivity toward CH_4 formation rather than C_2 species.

For the Co-Co_2C(1 0 1), CH species is the favored CH_x monomer, and CH self-coupling to C_2H_2 is much easier than the formation of CH_4 and C. Thus, the Co-Co_2C(1 0 1) is in favor of the formation of C_2 hydrocarbon C_2H_2 instead of C_2 oxygenate and C_1 hydrocarbon, which is also confirmed by the experimental studies [1,2,35] that Co_2C(1 0 1) surface

Table 3
All possible elementary reactions together with the corresponding activation free energy (ΔG_a/eV), reaction free energies (ΔG/eV) and effective barrier (E_{eff}/eV) at 493 K in the reactions related to CH_x(x = 1–3) species on the C- and Co-Co_2C(1 0 1) surfaces.

Reactions	C-Co_2C(1 0 1)			Co-Co_2C(1 0 1)		
	ΔG_a	ΔG	E_{eff}	ΔG_a	ΔG	E_{eff}
CH = C + H	1.27(1.26)	0.77(0.77)	1.40	0.53(0.52)*	−0.33(−0.34)*	1.02
CH + H = CH_2	0.41(0.30)	0.13(0.05)	0.45	0.91(0.92)	0.81(0.86)	1.20
CH + CH = C_2H_2	1.18(1.17)	−0.53(−0.52)	1.45	0.37(0.36)	0.22(0.21)	0.93
CH + CH_2 = CH_2CH	0.86(0.85)	−0.90(−0.88)	1.18	1.58(1.73)	0.57(0.72)	2.68
CH + CH_3 = CH_3CH	0.57(0.58)	−0.64(−0.59)	0.99	1.08(1.23)	0.48(0.63)	2.30
CH_2 = CH + H	0.28(0.25)	−0.13(−0.05)	0.44	0.10(0.06)	−0.81(−0.86)	0.73
CH_2 + H = CH_3	0.24(0.23)	−0.37(−0.33)	0.42	0.44(0.42)	0.07(0.13)	1.09
CH_2 + CH_2 = C_2H_4	0.42(0.41)	−0.92(−0.92)	0.78	0.73(0.74)	−0.25(−0.23)	2.09
CH_2 + CH_3 = CH_3CH_2	0.52(0.56)	−0.47(−0.42)	1.01	0.90(0.92)	0.12(0.15)	2.38
CH_3 = CH_2 + H	0.61(0.57)	0.37(0.33)	0.83	0.37(0.29)	−0.07(−0.13)	1.08
CH_3 + H = CH_4	0.37(0.40)	−0.45(−0.21)	0.67	0.69(0.76)	0.15(0.26)	1.54
CH_3 + CH_3 = C_2H_6	1.83(1.77)	0.52(0.66)	2.30	1.36(1.34)	0.08(0.17)	2.91
CH + CO = CHCO	0.68(0.64)	0.13(0.13)	0.79	0.93(0.90)	0.79(0.80)	1.20
CH_2 + CO = CH_2CO	0.60(0.60)	0.31(0.33)	0.79	0.99(0.98)	0.71(0.68)	1.66
CH_3 + CO = CH_3CO	0.94(0.95)	0.10(0.08)	1.22	1.18(1.21)	0.75(0.70)	2.00

* It is noted that values in the parentheses is at 0 K. n = 1 and 2 represent the transition states on the C-Co_2C(1 0 1) and Co-Co_2C(1 0 1) surfaces, respectively.

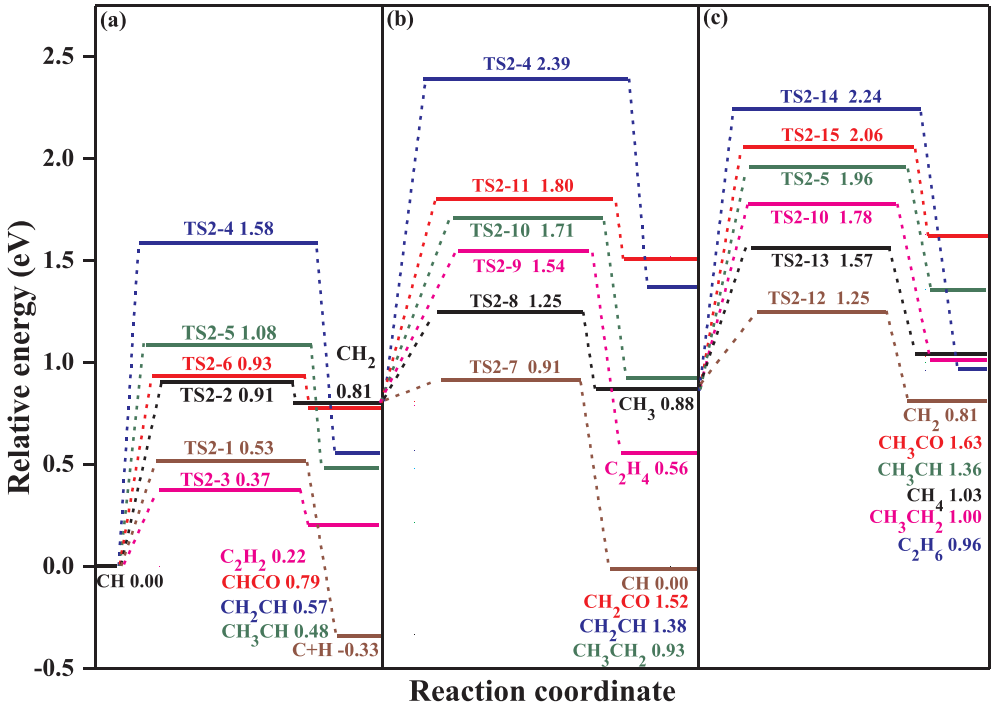

Fig. 4. The potential energy profile of Gibbs free energy (493 K) for the all reactions related to CH_x(x = 1–3) species on the Co-Co_2C(1 0 1) surface, the corresponding structures of initial states (ISs), transition states (TSs) and final states (FSs) are presented in Fig. 5.

has high selectivity of C_{2-4} hydrocarbons in FTS reactions.

Based on above results, it is concluded that the surface terminations of Co_2C(1 0 1) affect the existence form of favored CH_x monomer and the product selectivity of FTS reaction. The C- and Co-termination surfaces exhibit high selectivity toward the formation of CH_4 and C_2 hydrocarbons, respectively. Meanwhile, the previous experiment by Mohandas et al. [36] indicated that the initial FTS activity over bulk Co_2C yielded mostly CH_4 and CO_2, but as time progressed, CO conversion as well as the selectivity of higher hydrocarbons increased. Further, previous DFT studies by Li et al. [3] have investigated CO activation via the mechanism of the direct dissociation and hydrogen-assisted dissociation on the C- and Co-Co_2C(1 0 1) surfaces, indicating that CO hydrogen-assisted dissociation is energetically competitive with CO direct dissociation on the Co-Co_2C(1 0 1) surface (1.56 *vs.* 1.64 eV), while CO hydrogen-assisted dissociation is more favorable in kinetics than CO direct dissociation on the C-Co_2C(1 0 1) surface (2.04 *vs.* 2.49 eV). Namely, the Co-Co_2C(1 0 1) surface can provide the enough CH_x species for the carbon–carbon coupling reactions leading to the formation of C_2 hydrocarbons; whereas the C-Co_2C(1 0 1) surface is not favorable for CO activation to form CH_x species.

Therefore, taking above analysis and our calculation results into consideration, it is inferred that at the beginning stage of Co_2C formation, the Co_2C should expose the C-termination surface, which is in favor of surface C hydrogenation to CH_4 rather than CO activation to form CH_x species; with the process of the reaction, surface C atom is gradually eliminated by its hydrogenation to CH_4, until the Co-termination surfaces are exposed to promote CO activation to form CH_x species, followed by the formation of C_{2+} hydrocarbons via the coupling of CH_x species. Our results can provide a new explanation and evidence at a molecular level for the previous experiment results by

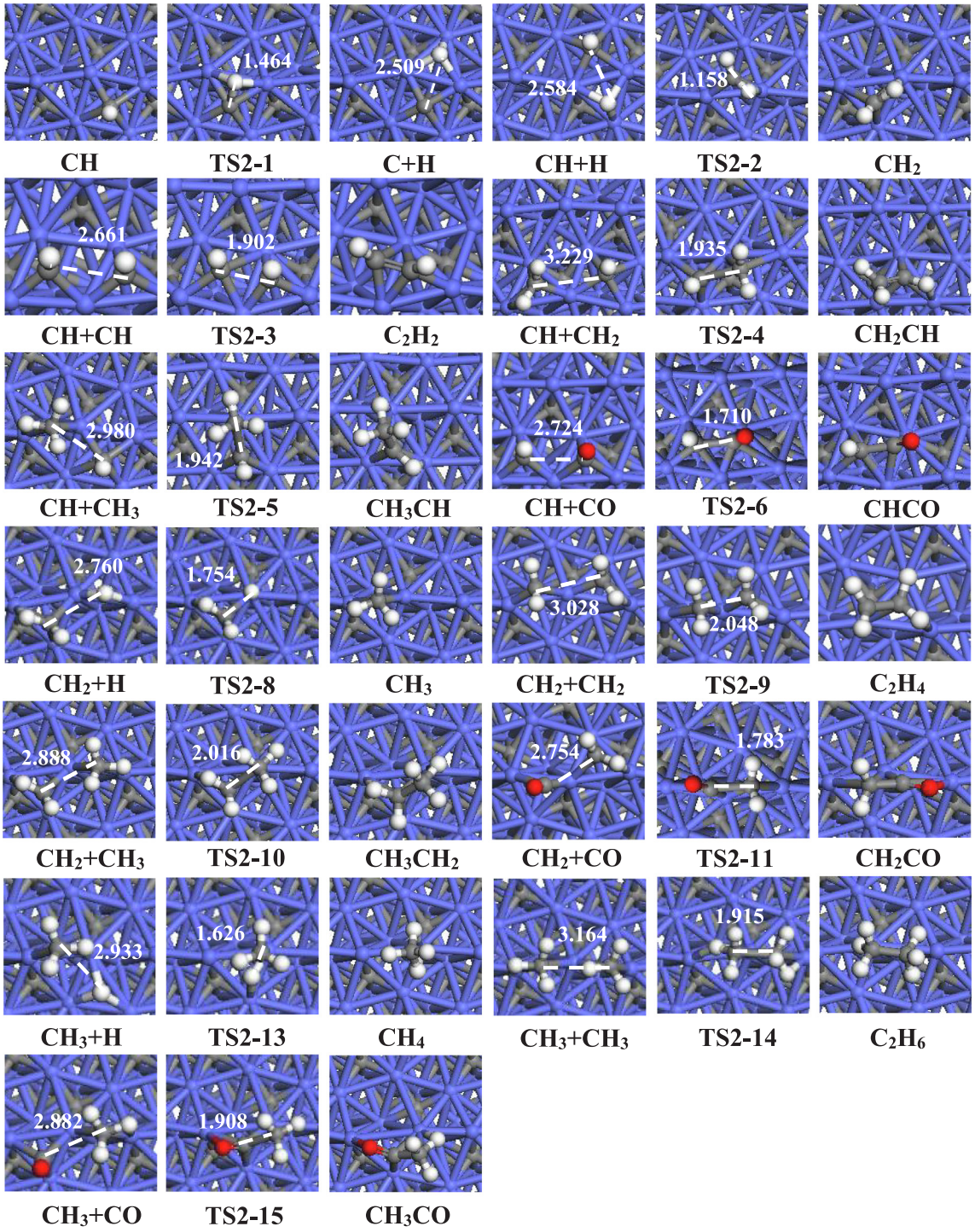

Fig. 5. The structures of initial states (ISs), transition states (TSs) and final states (FSs) for the all reactions related to CH_x(x = 1–3) species on the Co-Co_2C(1 0 1) surface. Co, C, H and O atoms are shown in the blue, grey, white and red balls, respectively. Bond length is in Å. (For interpretation of the references to colour in this figure legend, the reader is referred to the web version of this article.)

Mohandas et al. [36]. On the other hand, above results are also confirmed by the recent studies [37], in which the relationship between the coverage of carbon and the chemical potential of carbon over Co_2C(1 0 1) surfaces have been studied using the DFT calculations in combination with ab initio atomistic thermodynamics, suggesting that the chemical potential of carbon μ is crucial to the relative stability of different orientated surfaces and surface compositions of Co_2C. At higher μ, the C-rich surfaces are thermodynamically favorable, whereas at lower μ, the Co-rich surfaces could become thermodynamically favorable.

3.3.2. The analysis of surface electronic properties

In order to shed light on the essential difference between C- and Co-Co_2C(1 0 1) surfaces for FTS selectivity, we analyze the adsorption ability of C atom and CH_x(x = 1–3) species as well as the electronic properties of both Co_2C(1 0 1) surfaces.

It is well-known that the chemical bonding between an adsorbate and the metal surface controls the potential reactivity of adsorbate. If

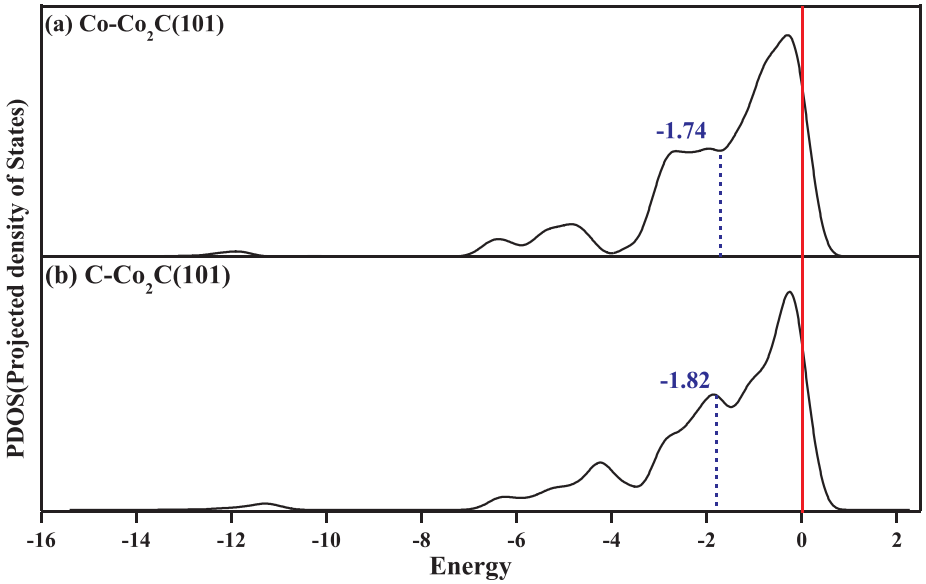

Fig. 6. Projected density of states (*p*DOS) for Co atoms over the (a) Co-Co_2C(1 0 1) and (b) C-Co_2C(1 0 1) surfaces. The blue dotted line indicates the *d*-band center; the red solid line denotes Fermi level. (For interpretation of the references to colour in this figure legend, the reader is referred to the web version of this article.)

the C and CH_x(x = 1–3) species binds weakly with the metal surface, its removal will cost less energy [17]. Thus, the less the adsorption energy of surface C and CH_x(x = 1–3) species is, the easier the formation of CH_4 is. Our results show that the adsorption ability of surface C and CH_x(x = 1–3) species over the C-termination surface is weaker than that over the Co-termination surface, thus, CH_4 formation is more favorable over the C-termination surface, which agrees with our kinetic results.

On the other hand, CH_x(x = 0–3) hydrogenation to CH_4 over Co_2C catalysts involves the successive insertion of H atom to Co-C bond. Previous studies about CH_x hydrogenation over Ni [38] and Fe_5C_2 [17,18,39] catalysts show that when the surface *d*-band center is far from the Fermi energy, this surface is more active for CH_x hydrogenation to CH_4. This is also confirmed by ethylene hydrogenation over Pd catalyst [40], and acetylene hydrogenation over Cu catalyst [41,42]. As shown in Fig. 6, the *d*-band center of C-Co_2C(1 0 1) surface (−1.82 eV) is far away from the Fermi level compared to that of Co-Co_2C(1 0 1) surface (−1.74 eV), suggesting that the C-Co_2C(1 0 1) surface prefers to promote CH_x hydrogenation to CH_4.

The average Bader charges of surface C and Co atoms over the C- and Co-Co_2C(1 0 1) surfaces are further analyzed, the electron of surface Co atom is +0.21 *e* over the Co-termination surface, whereas the electrons of surface C and Co atoms are −0.88 and +0.46 *e* over the C-termination surface, respectively, which agrees with the results by Li et al. [4]. Thus, the exposed surface C atoms of C-Co_2C(1 0 1) causes charge distribution non-uniform, as a result, Co atoms exhibit metallic properties, which enhances the catalytic activity of CH_x hydrogenation to CH_4.

For the formation of C_2 species, Fig. 7 demonstrates the potential energy profile for the most favorable pathways of CH_x coupling with CH_y to C_2H_{x+y} and CO insertion into CH_x to CH_xCO on the Co- and C-Co_2C(1 0 1) surfaces. On the C-Co_2C(1 0 1), the formation of C_2 hydrocarbons is always much easier than C_2 oxygenates in kinetics and thermodynamics, suggesting that C-Co_2C(1 0 1) has high activity and selectivity toward the formation of C_2 hydrocarbons than C_2 oxygenates; the same thing occurs over the Co-Co_2C(1 0 1) surface; thus, both C-Co_2C(1 0 1) and Co-Co_2C(1 0 1) surfaces are in favor of the formation of C_2 hydrocarbons instead of C_2 oxygenates. On the other hand, the differences of activation free energy between C_2 hydrocarbons and oxygenates for all related reactions of CH_x(x = 1–3) species over the Co-Co_2C(1 0 1) (0.56, 0.89 and 0.81 eV) are much larger than those over the C-Co_2C(1 0 1) (0.11, 0.36 and 0.37 eV). Namely, Co-Co_2C(1 0 1) exhibits higher selectivity toward the formation of C_2 hydrocarbons than C-Co_2C(1 0 1). Moreover, the activation free energy for the formation of C_2 hydrocarbons over Co-Co_2C(1 0 1) (0.37, 0.10, and 0.37 eV) is much lower than those over C-Co_2C(1 0 1) (0.57, 0.24 and 0.57 eV), suggesting that Co-Co_2C(1 0 1) presents higher catalytic activity toward the formation of C_2 hydrocarbons than C-Co_2C(1 0 1). Thus, the Co-Co_2C(1 0 1) surface presents higher catalytic activity and selectivity toward the formation of C_2 hydrocarbons, aiming at obtaining more C_{2+} hydrocarbons in Fischer-Tropsch synthesis, Co_2C catalyst should expose Co-termination surface under hydrogen-rich conditions; controlling the surface termination of Co_2C catalyst can adjust FTS selectivity toward the desirable products.

4. Conclusions

In this work, the effects of Co_2C(1 0 1) surface termination including the C- and Co-termination on the product selectivity of FTS have been systematically investigated using density functional theory calculations. The results show that on the C-termination surface, CH_3 is the favored CH_x monomer, CH_4 by CH_3 hydrogenation is the dominant C_1 species; whereas on the Co-termination surface, CH species is the favored CH_x monomer, CH self-coupling to C_2H_2 contributes to the dominant C_2 species. For the formation of C_2 species, both C- and Co-termination surfaces are in favor of C_2 hydrocarbons rather than C_2 oxygenates. Overall, Co_2C(1 0 1) surface exhibits higher selectivity toward the hydrocarbons instead of the oxygenates, in which the Co-termination surface corresponds to C_2 hydrocarbons and the C-termination surfaces is responsible for CH_4. Hence, controlling the surface termination of Co_2C catalysts can be an effective tool to adjust product selectivity of FTS reaction toward the most desirable products.

CRediT authorship contribution statement

Ping Liu: Data curation, Formal analysis, Investigation, Project administration, Writing - original draft, Writing - review & editing. **Danli Liang:** Methodology, Writing - review & editing. **Riguang Zhang:** Formal analysis, Methodology, Software. **Baojun Wang:** Conceptualization, Data curation, Funding acquisition, Project administration, Resources, Software, Supervision, Validation, Visualization.

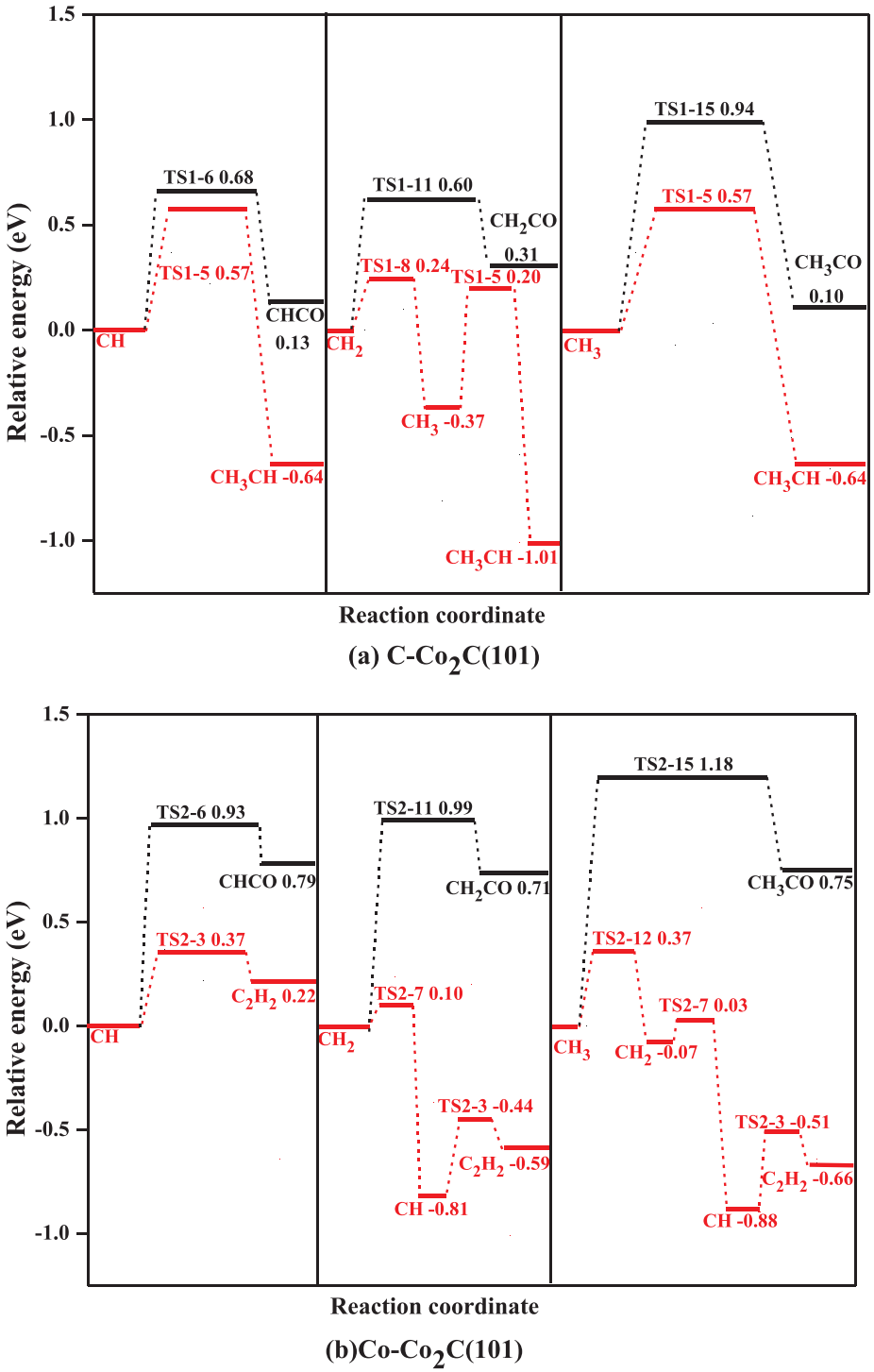

Fig. 7. The potential energy profile of the most favorable pathways for CH_x(x = 1–3) coupling to C_2H_y and CO insertion into CH_x to C_2H_xO on the (a) C-Co_2C(1 0 1), and (b) Co-Co_2C(1 0 1) surfaces.

Declaration of Competing Interest

The authors declare that they have no known competing financial interests or personal relationships that could have appeared to influence the work reported in this paper.

Acknowledgments

This work is financially supported by the National Natural Science Foundation of China (No. 21736007 and 21776193) and the Top Young Innovative Talents of Shanxi.

Appendix A. Supplementary data

The detailed descriptions for the Co_2C unit cell and the only one imaginary frequency corresponding to transition state, the methods for calculating the Gibbs free energy and the effective barriers are presented. Supplementary data to this article can be found online at https://doi.org/10.1016/j.commatsci.2019.109345.

References

[1] Z.J. Li, L.S. Zhong, F. Yu, Y.L. An, Y.Y. Dai, Y.Z. Yang, T.J. Lin, S.G. Li, H. Wang, P. Gao, Y.H. Sun, M.Y. He, Effects of sodium on the catalytic performance of CoMn catalysts for Fischer-Tropsch to olefin reaction, ACS Catal. 7 (2017) 3622–3631.

[2] L.S. Zhong, F. Yu, Y.L. An, Y.H. Zhao, Y.H. Sun, Z.J. Li, T.J. Lin, Y.J. Lin, X.Z. Qi, Y.Y. Dai, L. Gu, J.S. Hu, S.F. Jin, Q. Shen, H. Wang, Cobalt carbide nanoprisms for direct production of lower olefins from syngas, Nature 538 (2016) 84–87.

[3] W.D. Dong, J.X. Liu, H.J. Zhu, Y.J. Ding, Y.P. Pei, J. Liu, H. Du, M. Jiang, T. Liu, H.Y. Su, W.X. Li, Co-Co_2C and Co-Co_2C/AC catalysts for hydroformylation of 1–hexene under low pressure: experimental and theoretical studies, J. Phys. Chem. C 118 (2014) 19114–19122.

[4] Y.P. Pei, J.X. Liu, Y.H. Zhao, Y.J. Ding, T. Liu, W.D. Dong, H.J. Zhu, H.Y. Su, L. Yan, J.L. Li, W.X. Li, High alcohols synthesis via Fischer-Tropsch reaction at cobalt metal/carbide interface, ACS Catal. 5 (2015) 3620–3624.

[5] Y.H. Zhao, H.Y. Su, K.J. Sun, J.X. Liu, W.X. Li, Structural and electronic properties of cobalt carbide Co_2C and its surface stability: density functional theory study, Surf. Sci. 606 (2012) 598–604.

[6] Y.Z. Xiang, N. Kruse, Tuning the catalytic CO hydrogenation to straight- and long-chain aldehydes/alcohols and olefins/paraffins, Nat. Commun. 7 (2016) 13058.

[7] A.J. Medford, A. Vojvodic, F. Studt, F.A. Pedersen, J.K. Nørskov, Elementary steps of syngas reactions on Mo_2C(001): adsorption thermochemistry and bond dissociation, J. Catal. 290 (2012) 108–117.

[8] S.K. Kim, J. Kim, S.C. Lee, Surface-termination dependence of propanoic acid deoxygenation on Mo_2C, Catal. Commun. 99 (2017) 61–65.

[9] J. Ren, C.F. Huo, J.G. Wang, Y.W. Li, H.J. Jiao, Surface structure and energetics of oxygen and CO adsorption on α-Mo_2C(0001), Surf. Sci. 596 (2005) 212–221.

[10] X.R. Shi, J.G. Wang, K. Hermann, CO and NO adsorption and dissociation at the β-Mo_2C(0001) surface: a density functional theory study, J. Phys. Chem. C 114 (2010) 13630–13641.

[11] T. Wang, Y.W. Li, J.G. Wang, M. Beller, H.J. Jiao, High coverage CO adsorption and dissociation on the orthorhombic Mo_2C(100) Surface, J. Phys. Chem. C 118 (2014) 3162–3171.

[12] M. Huang, K. Cho, Density functional theory study of CO hydrogenation on a MoS_2 surface, J. Phys. Chem. C 113 (2009) 5238–5243.

[13] S.P. Pérez, F. Viñes, P.J. Ramirez, A.B. Vidal, J.A. Rodriguez, F. Illas, The bending machine: CO_2 activation and hydrogenation on δ-MoC(001) and β-Mo_2C(001) surfaces, Phys. Chem. Chem. Phys. 16 (2014) 14912–14921.

[14] Y.Y. Chen, M. Dong, Z.F. Qin, X.D. Wen, W.B. Fan, J.G. Wang, A DFT study on the adsorption and dissociation of methanol over MoS_2 surface, J. Mol. Catal. A: Chem. 338 (2011) 44–50.

[15] C.J. Orozco, E. Florez, A. Moreno, P. Liu, J.A. Rodriguez, Acetylene and ethylene adsorption on a β-Mo_2C(100) Surface: a periodic DFT study on the role of C- and Mo-terminations for bonding and hydrogenation reactions, J. Phys. Chem. C 121 (2017) 19786–19795.

[16] R.G. Zhang, G.X. Wen, H. Adidharma, A.G. Russell, B.J. Wang, M. Radosz, M.H. Fan, C_2 oxygenate synthesis via Fischer−Tropsch synthesis on Co_2C and Co/Co_2C interface catalysts: how to control the catalyst crystal facet for optimal selectivity, ACS Catal. 7 (2017) 8285–8295.

[17] C.F. Huo, Y.W. Li, J.G. Wang, H.J. Jiao, Insight into CH_4 formation in iron-catalyzed Fischer-Tropsch synthesis, J. Am. Chem. Soc. 131 (2009) 14713–14721.

[18] T.H. Pham, Y.Y. Qi, J. Yang, X.Z. Duan, G. Qian, X.G. Zhou, D. Chen, W.K. Yuan, Insights into Hägg iron-carbide-catalyzed Fischer−Tropsch synthesis: suppression of CH_4 formation and enhancement of C−C coupling on χ-Fe_5C_2(510), ACS Catal. 5 (2015) 2203–2208.

[19] G. Kresse, J. Hafner, Ab initio molecular-dynamics simulation of the liquid-metal-amorphous-semiconductor transition in germanium, Phys. Rev. B: Condens. Matter 49 (1994) 14251–14269.

[20] G. Kresse, J. Hafner, Ab initio molecular dynamics for liquid metals, Phys. Rev. B: Condens. Matter 47 (1993) 558–561.

[21] G. Kresse, J. Furthmüller, Efficient iterative schemes for ab initio total-energy calculations using a plane-wave basis set, Phys. Rev. B: Condens. Matter 54 (1996) 11169–11186.

[22] P.E. Blöchl, J. Kästner, C.J. Först, Electronic structure methods: augmented waves, pseudopotentials and the projector augmented wave method, Handbook of Materials Modeling, Springer, Netherlands, 2005, pp. 93–119.

[23] P.E. Blöchl, Projector augmented-wave method, Phys. Rev. B: Condens. Matter 50 (1994) 17953–17979.

[24] G. Kresse, D. Joubert, From ultrasoft pseudopotentials to the projector augmented-wave method, Phys. Rev. B: Condens. Matter 59 (1999) 1758–1775.

[25] J.A. White, D.M. Bird, Implementation of gradient-corrected exchange-correlation potentials in Car-Parrinello total-energy calculations, Phys. Rev. B: Condens. Matter 50 (1994) 4954–4957.

[26] J.P. Perdew, K. Burke, M. Ernzerhof, Generalized gradient approximation made simple, Phys. Rev. Lett. 77 (1996) 3865–3868.

[27] G. Henkelman, B.P. Uberuaga, H. Jónsson, A climbing image nudged elastic band method for finding saddle points and minimum energy paths, J. Chem. Phys. 113 (2000) 9901–9904.

[28] G. Henkelman, H. Jónsson, Improved tangent estimate in the nudged elastic band method for finding minimum energy paths and saddle points, J. Chem. Phys. 113 (2000) 9978–9985.

[29] G. Henkelman, H. Jónsson, A dimer method for finding saddle points on high dimensional potential surfaces using only first, J. Chem. Phys. 111 (1999) 7010–7022.

[30] K.J. Sun, Y.H. Zhao, H.Y. Su, W.X. Li, Force reversed method for locating transition states, Theor. Chem. Acc. 131 (2012) 1118.

[31] J. Cheng, X.Q. Gong, P. Hu, C.M. Lok, P. Ellis, S. French, A quantitative determination of reaction mechanisms from density functional theory calculations: Fischer-Tropsch synthesis on flat and stepped cobalt surfaces, J. Catal. 254 (2008) 285–295.

[32] S. Storsæter, D. Chen, A. Holmen, Microkinetic modelling of the formation of C_1 and C_2 products in the Fischer-Tropsch synthesis over cobalt catalysts, Surf. Sci. 600 (2006) 2051–2063.

[33] J. Cheng, P. Hu, P. Ellis, S. French, G. Kelly, C.M. Lok, Chain growth mechanism in Fischer-Tropsch synthesis: a DFT study of C−C coupling over Ru, Fe, Rh, and Re surfaces, J. Phys Chem. C 112 (2008) 6082–6086.

[34] J. Cheng, P. Hu, P. Ellis, S. French, G. Kelly, C.M. Lok, An energy descriptor to quantify methane selectivity in Fischer−Tropsch synthesis: a density functional theory study, J. Phys. Chem. C 113 (2009) 8858–8863.

[35] Z.J. Li, T.J. Lin, F. Yu, Y.L. An, Y.Y. Dai, S.G. Li, L.S. Zhong, H. Wang, P. Gao, Y.H. Sun, M.Y. He, Mechanism of Mn promoter via CoMn spinel for morphology control: formation of Co_2C nanoprisms for Fischer-Tropsch to olefins reaction, ACS Catal. 7 (2017) 8023–8032.

[36] J.C. Mohandas, M.K. Gnanamani, G. Jacobs, W.P. Ma, Y.Y. Ji, S. Khalid, B.H. Davis, Fischer-Tropsch synthesis: characterization and reaction testing of cobalt carbide, ACS Catal. 1 (2011) 1581–1588.

[37] P.P. Chen, J.X. Liu, W.X. Li, Carbon monoxide activation on cobalt carbide for Fischer−Tropsch synthesis from first-principles theory, ACS Catal. 9 (2019) 8093–8103.

[38] J.D. Li, E. Croiset, L.R. Sandoval, Methane dissociation on Ni(100), Ni(111), and Ni (553): a comparative density functional theory study, J. Mol. Catal. A: Chem. 365 (2012) 103–114.

[39] Y.W. Lu, R.G. Zhang, B.B. Cao, B.H. Ge, F.F. Tao, J.J. Shan, L. Nguyen, Z.H. Bao, T.P. Wu, J.W. Pote, B.J. Wang, F. Yu, Elucidating the copper–Hägg iron carbide synergistic interactions for selective CO hydrogenation to higher alcohols, ACS Catal. 7 (2017) 5500–5512.

[40] V. Pallassana, M. Neurock, Electronic factors governing ethylene hydrogenation and dehydrogenation activity of pseudomorphic Pd_{ML}/Re(0001), Pd_{ML}/Ru(0001), Pd (111), and Pd_{ML}/Au(111) surfaces, J. Catal. 191 (2000) 301–317.

[41] R.G. Zhang, B. Zhao, L.L. He, A.J. Wang, B.J. Wang, Cost-effective promoter-doped Cu-based bimetallic catalysts for the selective hydrogenation of C_2H_2 to C_2H_4: the effect of the promoter on selectivity and activity, Phys. Chem. Chem. Phys. 20 (2018) 17487–17496.

[42] R.G. Zhang, J. Zhang, Z. Jiang, B.J. Wang, M.H. Fan, The cost-effective Cu-based catalysts for the efficient removal of acetylene from ethylene: the effects of Cu valence state, surface structure and surface alloying on the selectivity and activity, Chem. Eng. J. 351 (2018) 732–746.